Surface displacements in the September 2005 Afar rifting event from satellite image matching: Asymmetric uplift and faulting

Ivana Barisin,[1] Sebastien Leprince,[2] Barry Parsons,[1] and Tim Wright[3]

Received 22 October 2008; revised 22 January 2009; accepted 23 January 2009; published 1 April 2009.

[1] Combining sub-pixel analysis of SPOT4 images with InSAR measurements, we generate 3D surface displacements for the September 2005 rifting event on the Dabbahu Segment in the Afar valley. The axis of rifting in the event is shifted to the east of the geomorphic rift. The horizontal displacements reveal 6 m of extension, and vertical displacements show asymmetric uplift of the flanks of the dike. Simple forward modelling indicates this asymmetry is due to the dike dipping 80° to the west towards the geomorphic rift. The boundary between eastward and westward displacements aligns with the transition between uplift and subsidence on the east in the north part of the segment, but on the west in the south. Normal faulting is not required on both sides of the instantaneous rift. East-dipping normal faulting on the west side of the instantaneous rift aligns with a west-dipping normal fault in the topography. **Citation:** Barisin, I., S. Leprince, B. Parsons, and T. Wright (2009), Surface displacements in the September 2005 Afar rifting event from satellite image matching: Asymmetric uplift and faulting, *Geophys. Res. Lett.*, *36*, L07301, doi:10.1029/2008GL036431.

1. Introduction and Setting

[2] The Afar triple junction is the junction of two seafloor spreading centres (the Red Sea and the Sheba Rift, Gulf of Aden) with the Main Ethiopian Rift, which is transitional from continental rifting to oceanic spreading and is located in the Afar depression. Divergence between the Arabian, Nubian and Somalian plates take place on these rifts (Figure 1a). The horizontal extension on the southern Red Sea Rift within the Afar depression has been localised on magmatic segments [*Hayward and Ebinger*, 1996]. These magmatic segments are formed by the injection of dikes into the upper crust from underlying magma chambers [*Ebinger et al.*, 2008].

[3] A large rifting episode in the northern Afar (Dabbahu Magmatic Segment) occurred in September 2005 during which 165 earthquakes were recorded, of which 15 were greater than M5, as well as a large vent opening associated with a small eruption [*Wright et al.*, 2006; *Rowland et al.*, 2007]. The purpose of this paper is to determine the surface displacements that occurred in the event through the matching of satellite images, and use these displacements to constrain models of the diking and normal faulting that produced them.

2. Three-Dimensional Surface Displacements

[4] After georeferencing and orthorectification, SPOT4 images acquired before and after dike intrusion (Table 1) should be identical, apart from the effect of surface displacements and a few remaining artifacts [see *Leprince et al.*, 2007]. Image correlation of two images within a sliding window in the Fourier domain has been shown to be capable of determining horizontal displacements at the subpixel level [*van Puymbroeck et al.*, 2000]. In the Fourier domain a horizontal displacement of the same function is reflected as a phase difference varying linearly with wave number [*Foroosh et al.*, 2002]. The phases are obtained by computing the normalized cross power spectrum of the Fourier transforms of the shifted images [*Hoge*, 2003]. An accurate subpixel displacement is obtained in the Fourier domain by minimizing the residuals between the computed normalized cross-spectrum and a predicted one [*Leprince et al.*, 2007].

[5] We first constructed a digital elevation model (DEM) (Figure 1b) from several 15 m Aster stereo-pair images (Table 1) using the ENVI AsterDTM module, which claims an accuracy of 20 m RMS in height. The individual DEMs were adjusted to the 90 m SRTM DEM and then mosaicked. Vertical differences between the ASTER and SRTM heights are in the range of 5–20 m. In addition to using this DEM as a ground reference for georeferencing the pre-event image, the DEM is used in the orthorectification of both images prior to the optical matching.

[6] Using the Co-registration of Optically Sensed Images and Correlation (COSI-CORR) software [*Ayoub and Leprince*, 2005; *Leprince et al.*, 2007], we georeferenced and orthorectified SPOT4-HRV1 images acquired before and after the rifting event (Table 1 and Figure S1).[1] Assuming that the only displacements between the two images are due to the rifting event, image correlation gives the E-W and N-S horizontal displacements (Figures 1c and 1d and Figures S2 and S3). We find that using a sliding window of 32 × 32 pixels with a 4-pixel step gives the best correlation results. The final spatial resolution of the displacement measurement maps is 40 m.

[7] The striped artifacts are most likely due to unmodelled spacecraft movements; we did not attempt to make any empirical corrections for these. The RMS variability of the far-field displacement observed for several areas of different sizes (Figure S2) is ~40 cm, and we infer that this represents the accuracy of the displacements. CCD mis-

[1] COMET, Department of Earth Sciences, University of Oxford, Oxford, UK.
[2] Division of Geological and Planetary Sciences, California Institute of Technology, Pasadena, California, USA.
[3] COMET, School of Earth and Environment, University of Leeds, Leeds, UK.

0094-8276/09/2008GL036431$05.00

[1] Auxiliary materials are available in the HTML. doi:10.1029/2008GL036431.

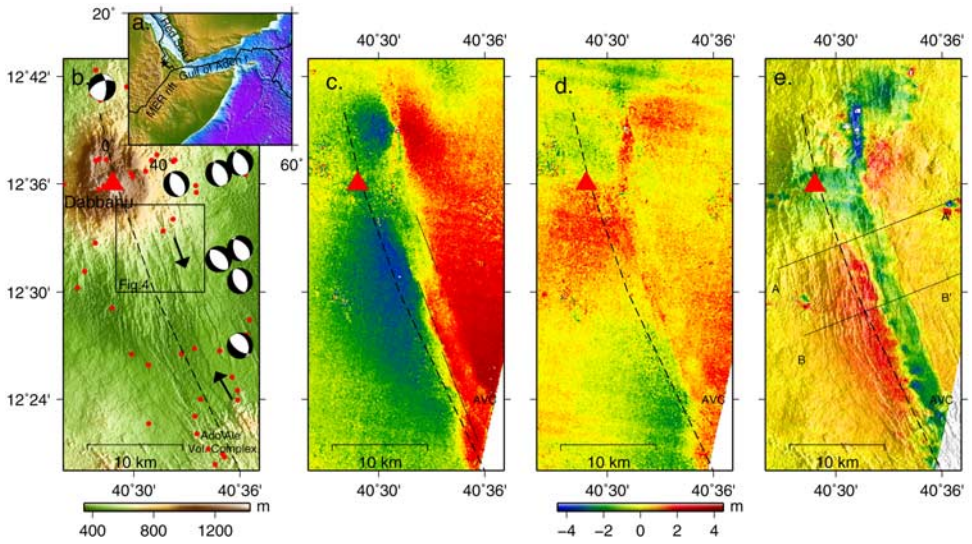

Figure 1. (a) The Afar Triple Junction. The black star shows the location of the area covered in Figures 1b–1e. (b) Shaded DEM generated from Aster images showing the area affected by the dike intrusion. Black arrows give the location of the new active dike. Focal mechanisms for earthquakes of M > 5 are the CMT solutions, and red circles are relocated earthquake epicenters from *Wright et al.* [2006]. The black dashed line shows the geomorphic rift axis. (c) East-west displacements from matching of SPOT4 images. Three black lines follow the location of the boundary between eastward and westward displacements. (d) North-south displacements from matching of SPOT4 images. (e) Vertical displacements derived from the E-W and N-S displacements and InSAR phase measurements. AA' and BB' profiles shown in Figure 3.

alignments of the SPOT4-HRV1 sensors were corrected as described by *Leprince et al.* [2008]. There are still some artifacts left from this misalignment to the far west of the images, but they do not affect the area of interest.

[8] A limitation of the optical matching method is that it yields only the horizontal components of the displacement. We calculated vertical displacements (Figures 1e and S6) by using the observed horizontal displacements to remove the contribution of the horizontal components to line-of-sight displacements from a SAR interferogram for the event [*Wright et al.*, 2004]. Here we use the descending interferogram (Figure S5) due to its greater spatial coverage, with any gaps in the interferogram filled with lower resolution and lower accuracy range-offset measurements [*Wright et al.*, 2006].

3. Interpretation of the Displacement Fields

[9] Horizontal displacements resolved perpendicular to the rift are shown in Figure 2a, and horizontal velocity vectors in Figure S3. The displacements show opening of the rift with a maximum extension of 6 m, which agrees well with the InSAR results [*Wright et al.*, 2006]. The location of the boundary between eastward and westward displacements switches from the eastern edge of the subsidence zone in the north to its western edge in the south (Figures 1c, 1e, 3, and S7).

[10] The vertical displacements in Figures 1e, 3, S6, and S7 show asymmetrical uplift of the rift flanks; the west flank uplifted ~1.5 m, while the east flank was uplifted ~1 m. Asymmetric uplift above dikes has been reported by other authors [e.g. *Sigmundsson et al.*, 1999]. The instantaneous rift as defined by the vertical displacements lies to the east of the topographic rift, along slightly raised topography (Figures 1e, 3, and S7), an observation made previously by *Rowland et al.* [2007]. We note that the location of the boundary of the vertical subsidence on the west side of the dike lies along the west-dipping normal fault seen in the topography. We measure a maximum subsidence of >4 m near the large vent reported by *Wright et al.* [2006], and an average of 1.5 m along the dike with a few areas that have subsided >2 m (Figure 1e).

[11] Sharp linear discontinuities in the E-W displacement map run parallel to some normal fault features in the topography (Figure 4) or large surface disturbances that appear visible in the imagery (Figure S8). Numerous linear features have been highlighted by running an edge filter (Figure S9), and we interpret these as the locations of active faulting or the opening of new fissures. The correlation quality map (Figure S4) shows a slight decorrelation (r = 0.98) in the area which aligns well with these features, presumably due to surface disturbances.

4. Modelling of the Rifting

[12] We focus only on diking and normal faulting events, leaving aside consideration of deflation of the volcanoes at the northern end of the segment. The location and strike of the dike and normal faults were fixed from the 3D displacement field and imagery. The displacements were forward

Table 1. Optical Satellite Images Used

	Image Date	Inc. Angle (deg)	Sun Azimuth (deg)	Sun Elevation (deg)
DEM generation	15.01.2001			
ASTER (15 m)	07.04.2005			
	20.05.2003			
	05.02.2006			
Image matching	19.12.2004	0.48	152	49.4
SPOT4 (10 m)	13.01.2006	−0.22	146	49.3

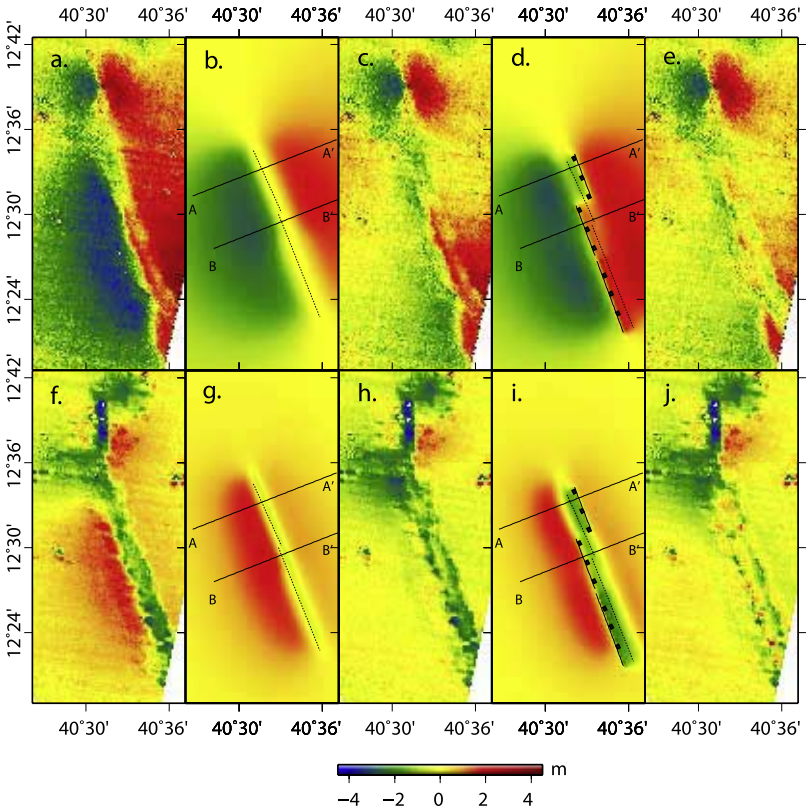

Figure 2. (a) Horizontal displacements perpendicular to the rift. (b) Model for extensional opening perpendicular to the rift computed including only the effects of a dike (dashed lines). (c) Residuals, (Figure 2a minus Figure 2b). (d) Model including both a dike and normal faults that are located as shown dipping towards the dike. (e) Residuals (Figure 2a minus Figure 2d). (f) Vertical displacements. (g) Vertical displacements predicted by model that includes only a dike. (h) Residuals (Figure 2f minus Figure 2g). (i) Vertical displacements of model that includes both a dike and normal faults. (j) Residuals (Figure 2f minus Figure 2i).

modelled as those due to tensile and shear dislocations in a homogeneous elastic half-space using the *Okada* [1985] formulation. By constraining the amount of opening from the surface deformation, we determined the bottom and top depth and the dip of the dike and faults assuming uniform movement on a rectangular plane.

[13] The vertical subsidence along the dike is ~2 km wide in the northern part and widens to ~2.5 km in the southern part. We divided the dike into two parts (Figures 2b and 2g) and modelled them separately. From the opening displacements perpendicular to the rift we measure 6 m extension at the surface, and referring to the results of the inversion of *Wright et al.* [2006], we fixed the opening on the dike to 8.5 m in the north part and 9 m in the south. The top depth of the dike, which controls the width of the rift at the surface, was then found to be 1.4 km in the north and 1.5 km in the south. The bottom depth of the dike, which determines the width of the uplift field, was found to be 5 km in the north and south.

[14] The asymmetry in vertical uplift on the flanks of the dike is best explained by having the dike plane dip at 80° to the west on both of the segments (Figures 3 and S7). Figures 2b and 2g show modeled horizontal displacements perpendicular to the rift and vertical displacements. The residuals between observed displacements and the model (Figures 2c and 2h) show that the model describes well the main characteristics of the extension and uplift outside the dike. The residuals for the vertical displacements also reveal more subsidence around the northern volcanos, making it a more circular shape (Figure 2h). We still observe areas of large residuals above the dike that are not sufficiently well explained by the model.

[15] *Rubin* [1992] showed that subsidence observed over dikes in Hawaii cannot be explained by the dikes alone, but required normal faulting to enhance the vertical displacement. We estimate that ~1.5 m of additional subsidence is needed here (Figures 2h and 3). Also a dike alone can not explain the switch in location of the transition between eastward and westward displacements along the rift. In contrast to *Wright et al.* [2006], who placed normal faults on each side of the dike, we fix the geometry in the north with one normal fault along the eastern subsidence boundary dipping west, and one normal fault in the south (split into two parts) along the western subsidence boundary dipping east (Figures 2d and 2i). These normal faults create a large component of subsidence above the dike and also explain a small amount of the extension. The profiles in Figures 3 and S7 show the improvements compared to the

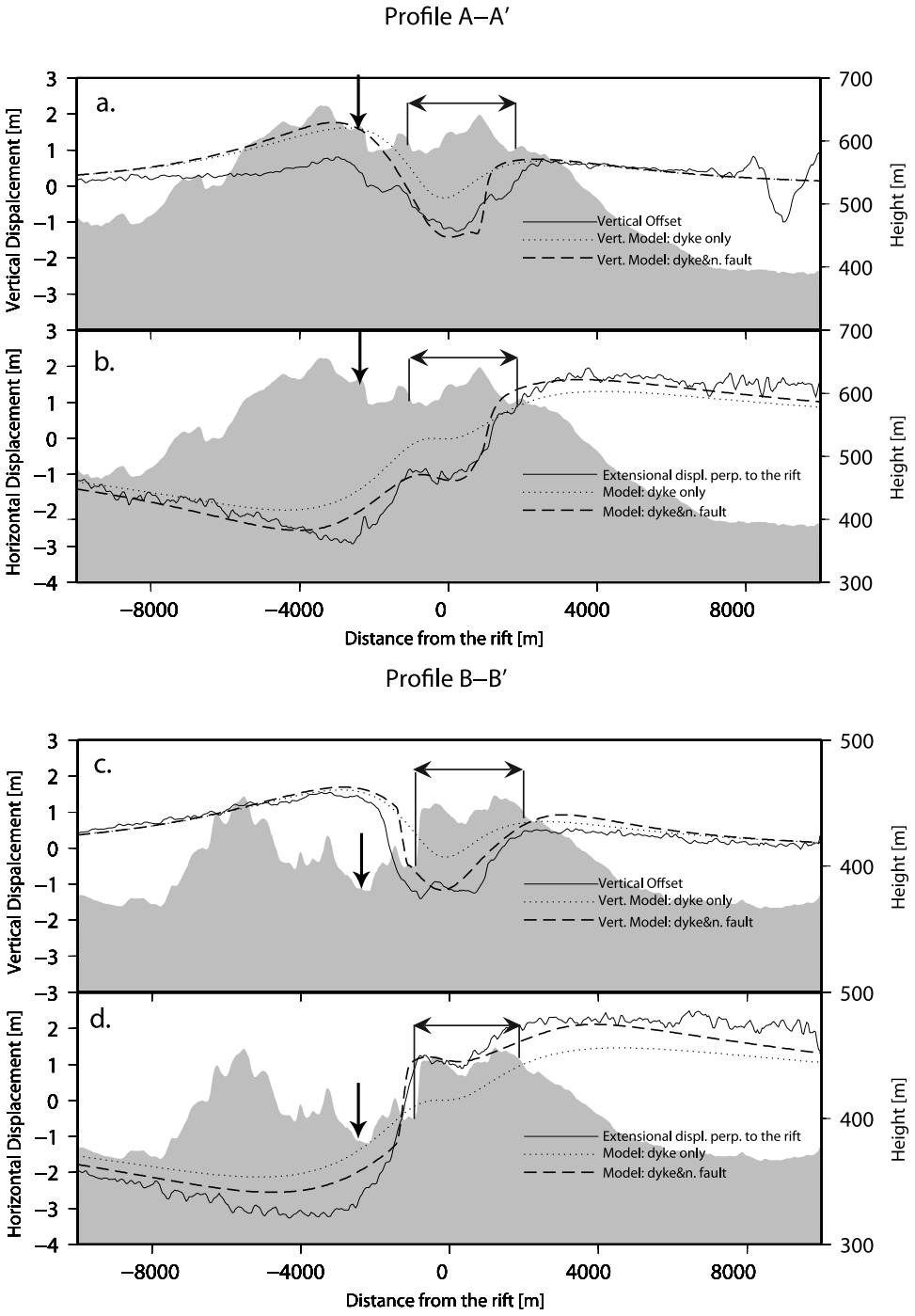

Figure 3. (a) and (c) Profiles of the derived vertical displacements and the predictions of the model with a dike element only and the model with a dike and normal faulting. (b) and (d) Profiles of the extensional displacements perpendicular to the rift and the predictions of a model using a dike only and a model using a dike and one normal fault. Gray color shows topographic profiles. Vertical arrows show the center of the geomorphic rift axis. Horizontal arrows show the extent of the new rifting event.

simple dike model. The residuals are shown in Figures 2e and 2j, and a summary of the parameters that we use to specify the model geometry is in Table 2.

5. Discussion

[16] The combination of image matching and InSAR has significantly improved the 3D deformation field previously constructed by *Wright et al.* [2006], highlighting the asymmetric deformation, a switch in the location of the transition between eastward and westward displacements, and the previously unknown locations of active faulting. A dike dipping to the west explains the asymmetry better than the vertical dike used in the model of *Wright et al.* [2006]. The observations are also explained better with a single normal fault on one or other side of the dike rather than two symmetrical conjugate normal faults.

[17] Further enhancement could be made by using a model with distributed instead of uniform slip on the dikes or faults. However, the RMS misfits in the far field outside the dike are already ~0.4 m or smaller. The remaining residuals within the subsiding zone, which includes some areas where the RMS of vertical misfit is ~0.8 m, are probably due to the complexities of the normal faulting geometry above the dike.

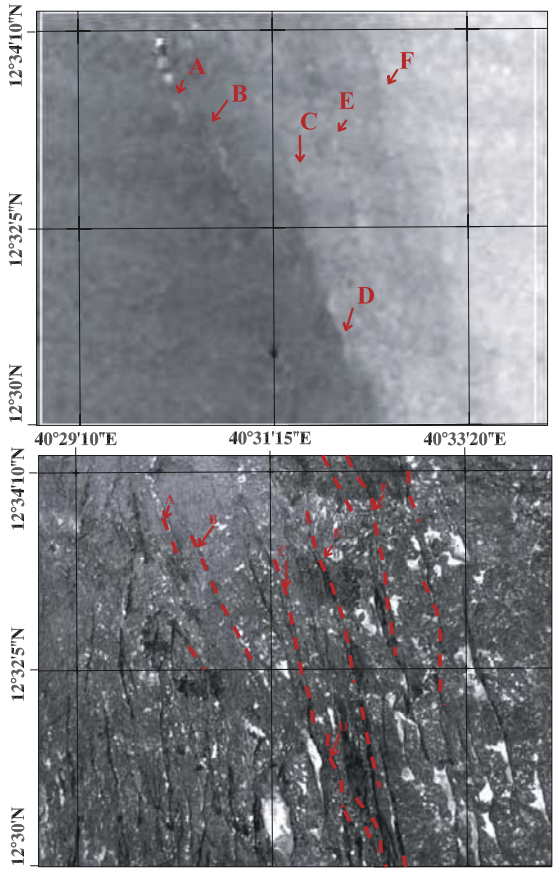

Figure 4. (a) Enlargement of the E-W displacement map with some linear discontinuities labelled A to F. (b) Portion of the orthophoto of the same geographical area as in Figure 4a. The linear discontinuities (the red lines) align well with the topographic features of the normal faults.

Table 2. Parameters Used to Fix the Model Geometry

	Opening (m)	Slip (m)	Dip (deg)	Strike (deg)	Top Depth (km)	Bottom Depth (km)	Length (km)
North Dike	8.5	0	80	158	1.4	5	12
South Dike	9	0	80	158	1.5	5	11
North Fault	0	3	40	160	0.1	2	6
Middle Fault	0	2.5	30	338	0.01	2	8
South Fault	0	3.8	30	340	0.05	2	10

[18] The results presented here raise many interesting questions. Is the shift in the instantaneous rift axis relative to the long-term geomorphic axis an unusual occurrence, or are all individual rifting events randomly distributed relative to the long-term axis? The westward dip of the dike in the model is consistent with a magmatic source to the west, perhaps beneath the topographic axis. Why is there a switch from west-dipping faulting in the north to east-dipping faulting in the south located where the images show a long-term west-dipping fault? This observation needs to be confirmed in the field.

[19] **Acknowledgments.** This research has been supported by the Natural Environment Research Council through the Centre for the Observation and Modelling of Earthquakes and Tectonics (COMET) and the National Centre for Earth Observation, and by the Royal Society through a fellowship to TW. SAR and SPOT data were provided by the European Space Agency. COSI-CORR was developed thanks to support from NSF grant EAR 0636097 and partial funding from the Gordon and Betty Moore Foundation. We are grateful for the advice of Jean-Philippe Avouac, who made possible the visits of IB and BP to the Tectonics Observatory at Caltech. We also thank Cindy Ebinger for sending us her paper before publication.

References

Ayoub, F., and S. Leprince (2005), *User's Guide to COSI-CORR v1.0 Co-registration of Optically Sensed Images and Correlation*, Calif. Inst. of Technol., Pasadena. (Available at www.tectonics.caltech.edu)

Ebinger, C., D. Keir, A. Ayele, E. Calais, T. Wright, M. Belachew, J. Hammond, M. Campbell, and R. Buck (2008), Capturing magma intrusion and faulting processes during continental rupture: Seismicity of the Dabbahu (Afar) rift, *Geophys. J. Int.*, *174*, 1138–1152, doi:10.1111/j.1365-246X.2008.03877.x.

Foroosh, H., J. Zerubia, and M. Berthod (2002), Extension of phase correlation to subpixel registration, *IEEE Trans. Image Process.*, *11*, 188–200, doi:10.1109/83.988953.

Hayward, N., and C. Ebinger (1996), Variations in the along-axis segmentations of the Afar rift system, *Tectonics*, *15*, 244–257.

Hoge, W. S. (2003), A subspace identification extension to the phase correlation method, *IEEE Trans. Med. Imaging*, *22*, 277–280, doi:10.1109/TMI.2002.808359.

Leprince, S., S. Barbot, F. Ayoub, and J.-P. Avouac (2007), Automatic and precise ortho-rectification, co-registration and sub-pixel correlation of satellite images, application to ground deformation measurements, *IEEE Trans. Geosci. Remote Sens.*, *45*, 1529–1558, doi:10.1109/TGRS.2006.888937.

Leprince, S., P. Muse, and J.-P. Avouac (2008), In-flight CCD distortion calibration for pushbroom satellites based on subpixel correlation, *IEEE Trans. Geosci. Remote Sens.*, *46*, 2675–2683, doi:10.1109/TGRS.2008.918649.

Okada, Y. (1985), Surface deformation due to shear and tensile faults in a half-space, *Bull. Seismol. Soc. Am.*, *75*, 1135–1154.

Rowland, J., E. Baker, C. Ebinger, D. Keir, T. Kidane, J. Biggs, N. Hayward, and T. Wright (2007), Fault growth at a nascent slow-spreading ridge: 2005 Dabbahu rifting episode, Afar, *Geophys. J. Int.*, *442*, 1226–1246, doi:10.1111/j.1365-246X.2007.03584.x.

Rubin, A. (1992), Dike-induced faulting and graben subsidence in volcanic rift zones, *J. Geophys. Res.*, *97*, 1839–1858.

Sigmundsson, F., P. Durand, and D. Massonnet (1999), Opening of an eruptive fissure and seaward displacement at Piton de la Fournaise volcano measured by radarsat satellite radar interferometry, *Geophys. Res. Lett.*, *26*, 533–536.

van Puymbroeck, N., R. Michel, R. Binet, J.-P. Avouac, and J. Taboury (2000), Measuring earthquakes from optical satellite images, *Appl. Opt.*, *39*, 3486–3494.

Wright, T. J., B. E. Parsons, and Z. Lu (2004), Toward mapping surface deformation in three dimensions using InSAR, *Geophys. Res. Lett.*, *31*, L01607, doi:10.1029/2003GL018827.

Wright, T., C. Ebinger, J. Biggs, A. Ayele, G. Yirgu, D. Keir, and A. Stork (2006), Magma-maintained rift segmentation at continental rupture in the 2005 Afar dyking episode, *Nature*, *442*, 291–294, doi:10.1038/nature04978.

I. Barisin and B. Parsons, COMET, Department of Earth Sciences, University of Oxford, Oxford OX1 3PR, UK. (ivanab.earth.ox.ac.uk)

S. Leprince, Division of Geological and Planetary Sciences, California Institute of Technology, Pasadena, CA 91125, USA.

T. Wright, COMET, School of Earth and Environment, University of Leeds, Leeds LS2 9JT, UK.